Published in final edited form as:
Science. 2016 October 20; 354(6310): 305–307. doi:10.1126/science.aah5974.

Molecular force spectroscopy with a DNA-origami–based nanoscopic force clamp

Philipp C. Nickels[1], **Bettina Wünsch**[2], **Phil Holzmeister**[2,†], **Wooli Bae**[1], **Luisa M. Kneer**[1], **Dina Grohmann**[2,‡], **Philip Tinnefeld**[2,*], and **Tim Liedl**[1,*]

[1]Faculty of Physics & Center for Nanoscience (CeNS), Ludwig-Maximilians-Universität (LMU), Geschwister-Scholl-Platz 1, 80539 München, Germany

[2]Institut für Physikalische und Theoretische Chemie, and Braunschweig Integrated Centre of Systems Biology (BRICS), and Laboratory for Emerging Nanometrology (LENA), Technische Universität Braunschweig, Rebenring 56, 38106 Braunschweig, Germany

Abstract

Forces in biological systems are typically investigated at the single-molecule level with atomic force microscopy or optical and magnetic tweezers, but these techniques suffer from limited data throughput and their requirement for a physical connection to the macroscopic world. We introduce a self-assembled nanoscopic force clamp built from DNA that operates autonomously and allows massive parallelization. Single-stranded DNA sections of a DNA origami structure acted as entropic spring and exerted controlled tension in the low piconewton range to a molecular system, whose conformational transitions were monitored via single-molecule Förster resonance energy transfer. We used the conformer switching of a Holliday junction as a benchmark and studied the TATA-binding protein-induced bending of a DNA duplex under tension. The observed suppression of bending above 10 pN provides further evidence of mechano-sensitivity in gene regulation.

The most widely used single-molecule force spectroscopy techniques to study minute forces and mechanical properties of biomolecules are atomic force microscopy and optical or magnetic tweezers. These methods helped to explore the unfolding and folding of proteins (1, 2), the elasticity of DNA (3), and the folding trajectory of proteins in force clamp configurations (4). Despite this great success, two limitations persist. One is the low data throughput arising from the serial nature of conventional force spectroscopy. Recent

*Correspondence to: p.tinnefeld@tu-braunschweig.de, tim.liedl@physik.lmu.de.
†Current address: Bayer AG, Engineering & Technology, Enabling Technologies, Chempark E41, 51368 Leverkusen, Germany
‡Current address: Department of Biochemistry, Genetics and Microbiology, Institute of Microbiology, University of Regensburg, 93053 Regensburg, Germany

Author contributions:
P.N., B.W. and P.H. performed the experiments. P.N., D.G., P.T. and T.L. designed the research. P.N., B.W., P.H., L.K., W.B., P.T. and T.L. analyzed the data. P.N. and W.B. prepared the figures. P.N., P.T., D.G. and T.L. wrote the manuscript. All authors edited the manuscript.

Competing interests:
The authors declare that they have no competing interests.

Data and materials availability:
Additional data described in this work can be found in the online supplementary materials.

attempts to overcome this problem include the development of increased parallel data acquisition in magnetic tweezer experiments (6) and centrifuge force microscopes (7). The second limitation is the requirement of a physical connector to a micrometer-sized object that enables interaction with the macroscopic world (5). These typically long and flexible connector molecules are an intrinsic feature of all established techniques and make them susceptible to drift and noise. Further, they prevent the investigation of DNA interacting systems that induce only minor conformational changes, such as many gene regulatory proteins, e.g. transcription factors. One previous attempt to reduce noise is the construction of DNA origami bundles as rigid spacers in optical traps (8). Regardless, any tether prohibits access to biologically relevant complex environments such as the inside of living cells.

A promising approach toward the complete removal of the invasive connection is the construction of autonomous, nanoscopic manipulation tools. Earlier efforts on the molecular scale to sense forces autonomously, although not in an adjustable fashion, include simple nanomechanical DNA devices (9–11) and intracellular protein force sensors (12). Here, we use programmable DNA self-assembly (13–18) to construct a nanoscopic device that overcomes both limitations. Extending pre-stressed DNA origami tensegrity (19), we use the entropic spring behavior of single-stranded DNA (ssDNA) to exert defined and tunable forces on molecular systems. Conceptually, the ssDNA connects the system of interest with two immobile anchor points (Fig. 1A). By adjusting the number of bases between the fixed anchor points, the contour length of the ssDNA is changed, directly affecting the entropic force acting on the system under study. The fixed distance imparted by the rigid DNA structure and the given contour length of the ssDNA provide an approximately constant force over time (also see supplementary text S1) (20). In analogy to the nomenclature of established constant force experiments, we call our device a nanoscopic force clamp.

In the experimental realization, the ssDNA spring spans the gap of a rigid, bracket-shaped DNA origami clamp and is part of the long scaffold strand that forms the backbone of the DNA origami structure (Fig. 1B). For our design, we located the multiple cloning site (MCS) of the M13mp18 scaffold in the middle of the spring, which allowed us to insert and probe any DNA sequence of interest via standard cloning procedures. Additional ssDNA scaffold was stored in reservoir loops on both ends of the clamp. This enabled us to cost-efficiently build multiple objects with ssDNA springs of different lengths, providing a flexible design with adjustable force (19). Individual structures were assembled for each chosen length of the ssDNA spring with a unique subset of only ten oligonucleotides (staple strands) (Fig. 1C and figs. S1 to S3). For a zero force control, we enzymatically cut the single-stranded spring to release any tension from the region of interest (Fig 1C).

To calculate the resulting force for a given contour length, we approximated the ssDNA as a purely entropic spring using a modified freely-jointed-chain model (3) with the contour length $L_C = N^* L_B$ with N being the number of nucleotides and L_B the length per single base (supplementary text S1). For L_B we used 6.3 Å ± 0.8 Å from a length comparison of five different crystal structures of ssDNA segments (21).

We thermally annealed the force clamp structure, providing ~ 10^{12} force clamps in a single one-pot reaction. The chosen annealing ramp avoided temperatures above 65°C to minimize

thermal degradation of the scaffold (fig. S4 and supplementary text S2) (20). We confirmed successful assembly via agarose gel electrophoresis (Fig. 1D and fig. S5), bulk FRET experiments (fig. S6) and transmission electron microscopy (TEM) (Fig. 1E and figs. S7 to S13).

To demonstrate the functionality and sensitivity of our force clamp, we cloned a sequence into the scaffold that, together with three other oligonucleotides, forms the well-studied four-way Holliday junction (HJ) (22). In the presence of magnesium, the HJ forms an X-like structure by pairwise coaxial stacking of its helical arms. The chosen sequence is known to constantly switch between the two stacking conformers *iso* I and *iso* II (Fig. 2A) (22), a process that can be efficiently monitored with the help of a donor-acceptor FRET pair positioned on two of the arms (Fig. 2B and fig. S14). We chose four force variants ranging from 0 pN to 4.0 pN and confirmed their successful assembly (figs. S15 to S23). We immobilized these structures on a coverslip surface and monitored donor- and acceptor-pair intensities from individual force clamps over time in a confocal single-molecule setup with alternating laser excitation (ALEX) (20, 23).

Figure 2C and 2D show exemplary FRET traces and FRET histograms from thousands of transitions for each constant force experiment (more traces in figs. S24 and S25). A low FRET population was centered at the FRET efficiency $E = 0.42$ (corresponding to *iso* I) and a FRET population at $E = 0.85$ (corresponding to *iso* II). With increasing force, the equilibrium shifted toward the *iso* II conformation with almost zero low-FRET population left at 4.0 pN. We used two-state hidden Markov modeling (24) to calculate the transition rates between the low- and high-FRET conformations for each of the forces. The transition rate from low- to high-FRET (k_{high}) increased from 4.7 s^{-1} ± 0.4 s^{-1} at 0 pN to 18.3 s^{-1} ± 1.4 s^{-1} at 4.0 pN. Meanwhile, the rate from high- to low-FRET (k_{low}) decreased from 3.2 s^{-1} ± 0.6 s^{-1} at 0 pN to 1.7 s^{-1} ± 0.4 s^{-1} at 4.0 pN (Fig. 2E). These rate changes are in good agreement with reported values from combined FRET and optical- and magnetic-tweezer measurements (22, 25). Importantly, the heterogeneity of the HJ (26) was preserved in our measurements (fig. S26), indicating that the force clamp itself did not influence the dynamics of the HJ.

Next, we studied the force dependency of the TATA-binding protein (TBP) induced bending of a DNA duplex. Such DNA distortions are an integral function of many transcription factors and DNA binding proteins. Although the correlation between transcriptional regulation and chromosome organization is well known, it has been challenging to quantify the impact of the DNA condensation state and the chromosome organization (e.g. the extent of strain in the DNA) on transcription factors such as TBP.

The general transcription factor TBP is found in the archaeal and eukaryotic domain of life. It recognizes the minor groove of the adenine- and thymidine-rich TATA-box in the core promotor sequence and introduces a severe bend of ~ 90° in the DNA. Together with transcription factor B (TFB/TF(II)B), TBP is responsible for the site-specific recruitment and orientation of RNA polymerases at the transcription start site. To date, force measurements of this system have been futile, at least partly because the TBP-induced changes in the DNA topology are not easily detectable through the long tethers that are

unavoidable in standard force spectroscopy experiments. Fluorescence readout in combination with our high throughput method helped us to circumvent this problem.

We used TBP from the hyperthermophilic archaeal organism *Methanocaldococcus jannaschii* (MjTBP) (Fig. 3A), which bends the promotor DNA in a one-step bending mechanism without the need for the second transcription initiation factor TFB/TF(II) (27), and inserted a promoter sequence (derived from the Sulfolobus spindle-shaped virus 1 (SSV) T6 gene promoter), which contains a TATA-box motif and is recognized by MjTBP, into the scaffold (Fig. 3B and fig. S27). We chose six force clamp variants ranging from 0 pN to 11.4 pN and confirmed their successful assembly (figs. S28 to S40). The complementary strand of the 51 base pair long SSV T6 promotor was hybridized to the scaffold during folding. Bending was monitored by single-molecule FRET via a donor-acceptor pair flanking the TATA-box (Fig. 3C and fig. S27). Here, we chose in-solution over surface measurements to drastically increase the data acquisition throughput (28). Fluorescence bursts of donor and acceptor were recorded before and after the addition of MjTBP.

Figure 3D shows the FRET efficiency histograms with MjTBP for the six different forces. Each histogram includes at least 10,000 measured force clamps, although the average recording time per sample was only ~ 30 min. All histograms showed a bimodal distribution with a low-FRET population centered at $E = 0.42$ (corresponding to the undistorted state) and a high-FRET population centered at $E = 0.74$ (corresponding to the bent state). The high FRET population disappeared gradually with increasing force and the TBP-induced bending was almost completely suppressed at 11.4 pN (full E - S histograms in fig. S41). We calculated the probability of the bent state P_{bent} via its relative occurrence within the bimodal FRET distribution and plotted P_{bent} as a function of force (Fig. 3E). P_{bent} is well described by the free energy difference of the unbent and bent state expressed through a Boltzmann distribution (Fig. 3E and supplementary text S3) (20). An estimate of the change in binding affinity and Gibbs free energy is given in fig. S42.

The presented DNA origami force clamp provides a new tool to quantify the sensitivity of transcription factor-induced distortion to DNA tension and thus to chromosome organization. This adds new information to the growing picture of transcriptional regulation and protein-DNA interactions in general. Our nanoscopic force clamp expands the range of available single-molecule force spectroscopy techniques and makes new molecular systems accessible to sensitive force spectroscopy analysis. The self-assembling clamps are easy to prepare and can be used to study any DNA-interacting and DNA-modifiable system, e.g. proteins conjugated with short DNA tethers. Simple operation and highly increased throughput compared to standard techniques facilitate the generation of force spectroscopy data with a dynamic range of 0 to 12 pN, which easily can be extended to ~ 50 pN (supplementary text S4) (20). As our method provides the flexibility to perform both on-surface and in-solution experiments, we further envision moving from elaborate and costly single-molecule tools toward simple and readily adaptable ensemble assays.

Supplementary Material

Refer to Web version on PubMed Central for supplementary material.

Acknowledgments

We thank Hermann Gaub, Andreas Gietl, Alexander Maier, Iain MacPherson, Jan Lipfert, Mauricio Pilo-Pais, Joachim Rädler, Omar Saleh, and Tao Zhang for discussions and Susanne Kempter and Gerlinde Schwake for technical assistance. Sarah Schulz kindly prepared the MjTBP.

Funding:

This work was supported by the Deutsche Forschungsgemeinschaft (LI 1743/2-1, TI 329/6-1, GrK1952/1 'Metrology for Complex Nanosystems', Nanosystems Initiative Munich, SFB 1032 (TPA6) and SFB 960 (TPA7)), the Braunschweig International Graduate School of Metrology B-IGSM, the European Commission (FP7 - EScoDNA GA no. 317110 and ERC grant agreement n° 336440, ORCA), and the Boehringer Ingelheim Foundation.

References

1. Kellermayer MS, Smith SB, Granzier HL, Bustamante C. Folding-unfolding transitions in single titin molecules characterized with laser tweezers. Science. 1997; 276:1112–1116. [PubMed: 9148805]
2. Rief M, Gautel M, Oesterhelt F, Fernandez JM, Gaub HE. Reversible unfolding of individual titin immunoglobulin domains by AFM. Science. 1997; 276:1109–1112. [PubMed: 9148804]
3. Smith SB, Cui Y, Bustamante C. Overstretching B-DNA: the elastic response of individual double-stranded and single-stranded DNA molecules. Science. 1996; 271:795–799. [PubMed: 8628994]
4. Fernandez JM, Li H. Force-clamp spectroscopy monitors the folding trajectory of a single protein. Science. 2004; 303:1674–1678. [PubMed: 15017000]
5. Neuman KC, Nagy A. Single-molecule force spectroscopy: optical tweezers, magnetic tweezers and atomic force microscopy. Nat Meth. 2008; 5:491–505.
6. Ribeck N, Saleh OA. Multiplexed single-molecule measurements with magnetic tweezers. Rev Sci Instrum. 2008; 79
7. Halvorsen K, Wong WP. Massively parallel single-molecule manipulation using centrifugal force. Biophys J. 2010; 98:L53–5. [PubMed: 20513382]
8. Pfitzner E, et al. Rigid DNA Beams for High-Resolution Single-Molecule Mechanics. Angew Chem Int Ed. 2013; 52:7766–7771.
9. Shroff H, et al. Biocompatible Force Sensor with Optical Readout and Dimensions of 6 nm ^{3}. Nano Lett. 2005; 5:1509–1514. [PubMed: 16178266]
10. Shen W, Bruist MF, Goodman SD, Seeman NC. A Protein-Driven DNA Device That Measures the Excess Binding Energy of Proteins That Distort DNA. Angew Chem Int Ed. 2004; 43:4750–4752.
11. Gu H, Yang W, Seeman NC. DNA scissors device used to measure MutS binding to DNA mis-pairs. J Am Chem Soc. 2010; 132:4352–4357. [PubMed: 20205420]
12. Grashoff C, et al. Measuring mechanical tension across vinculin reveals regulation of focal adhesion dynamics. Nature. 2010; 466:263–266. [PubMed: 20613844]
13. Seeman N. DNA in a material world. Nature. 2003; 421:427–431. [PubMed: 12540916]
14. Rothemund PWK. Folding DNA to create nanoscale shapes and patterns. Nature. 2006; 440:297–302. [PubMed: 16541064]
15. Douglas SM, et al. Rapid prototyping of 3D DNA-origami shapes with caDNAno. Nucleic Acids Res. 2009; 37:5001–5006. [PubMed: 19531737]
16. Ke Y, et al. Multilayer DNA origami packed on a square lattice. J Am Chem Soc. 2009; 131:15903–15908. [PubMed: 19807088]
17. Andersen ES, et al. Self-assembly of a nanoscale DNA box with a controllable lid. Nature. 2009; 459:73–76. [PubMed: 19424153]
18. Douglas SM, et al. Self-assembly of DNA into nanoscale three-dimensional shapes. Nature. 2009; 459:414–418. [PubMed: 19458720]
19. Liedl T, Högberg B, Tytell J, Ingber DE, Shih WM. Self-assembly of three-dimensional prestressed tensegrity structures from DNA. Nat Nanotechnol. 2010; 5:520–524. [PubMed: 20562873]
20. Materials and methods are available as supplementary materials on *Science* Online.

21. Murphy MC, Rasnik I, Cheng W, Lohman TM, Ha T. Probing single-stranded DNA conformational flexibility using fluorescence spectroscopy. Biophys J. 2004; 86:2530–2537. [PubMed: 15041689]
22. Hohng S, et al. Fluorescence-force spectroscopy maps two-dimensional reaction landscape of the holliday junction. Science. 2007; 318:279–283. [PubMed: 17932299]
23. Ross J, et al. Multicolor Single-Molecule Spectroscopy with Alternating Laser Excitation for the Investigation of Interactions and Dynamics. J Phys Chem B. 2007; 111:321–326. [PubMed: 17214479]
24. McKinney SA, Joo C, Ha T. Analysis of Single-Molecule FRET Trajectories Using Hidden Markov Modeling. Biophys J. 2006; 91:1941–1951. [PubMed: 16766620]
25. Kemmerich FE, et al. Simultaneous Single-Molecule Force and Fluorescence Sampling of DNA Nanostructure Conformations Using Magnetic Tweezers. Nano Lett. 2016; 16:381–386. [PubMed: 26632021]
26. Hyeon C, Lee J, Yoon J, Hohng S, Thirumalai D. Hidden complexity in the isomerization dynamics of Holliday junctions. Nat Chem. 2012; 4:907–914. [PubMed: 23089865]
27. Gietl A, et al. Eukaryotic and archaeal TBP and TFB/TF(II)B follow different promoter DNA bending pathways. Nucleic Acids Res. 2014; 42:6219–6231. [PubMed: 24744242]
28. Kapanidis AN, et al. Alternating-laser excitation of single molecules. Acc Chem Res. 2005; 38:523–533. [PubMed: 16028886]
29. Adachi N, Senda M, Natsume R, Senda T, Horikoshi M. Crystal structure of Methanococcus jannaschii TATA box-binding protein. Genes to Cells. 2008; 13:1127–1140. [PubMed: 19090808]
30. Sambrook, J, Russell, DW. Molecular cloning: a laboratory manual. ed. 3. CSHL Press; Cold Spring Harbour, NY: 2001.
31. Douglas SM, Chou JJ, Shih WM. DNA-nanotube-induced alignment of membrane proteins for NMR structure determination. Proc Natl Acad Sci U S A. 2007; 104:6644–6648. [PubMed: 17404217]
32. Stahl E, Martin TG, Praetorius F, Dietz H. Facile and Scalable Preparation of Pure and Dense DNA Origami Solutions. Angew Chem Int Ed. 2014; 53:12735–12740.
33. de la Rosa-Trevín JM, et al. Xmipp 3.0: an improved software suite for image processing in electron microscopy. J Struct Biol. 2013; 184:321–328. [PubMed: 24075951]
34. Ha T, Tinnefeld P. Photophysics of fluorescent probes for single-molecule biophysics and super-resolution imaging. Annu Rev Phys Chem. 2012; 63:595–617. [PubMed: 22404588]
35. Nir E, et al. Shot-noise limited single-molecule FRET histograms: comparison between theory and experiments. J Phys Chem B. 2006; 110:22103–22124. [PubMed: 17078646]
36. Tomov TE, et al. Disentangling Subpopulations in Single-Molecule FRET and ALEX Experiments with Photon Distribution Analysis. Biophys J. 2012; 102:1163–1173. [PubMed: 22404939]
37. Strobl, GR. The Physics of Polymers. ed. 3. Springer Science & Business Media; Berlin Heidelberg, Germany: 2007.
38. McIntosh DB, Saleh OA. Salt Species-Dependent Electrostatic Effects on ssDNA Elasticity. Macromolecules. 2011; 44:2328–2333.
39. Zimm BH. Dynamics of Polymer Molecules in Dilute Solution: Viscoelasticity, Flow Birefringence and Dielectric Loss. J Chem Phys. 1956; 24:269–11.
40. Strunz T, Oroszlan K, Schafer R, Guntherodt HJ. Dynamic force spectroscopy of single DNA molecules. Proc Natl Acad Sci U S A. 1999; 96:11277–11282. [PubMed: 10500167]

Europe PMC Funders Author Manuscripts

Europe PMC Funders Author Manuscripts

One Sentence Summary

A self-assembled molecular force clamp built from DNA allows highly parallelized force spectroscopy measurements without interference from the macroscopic world.

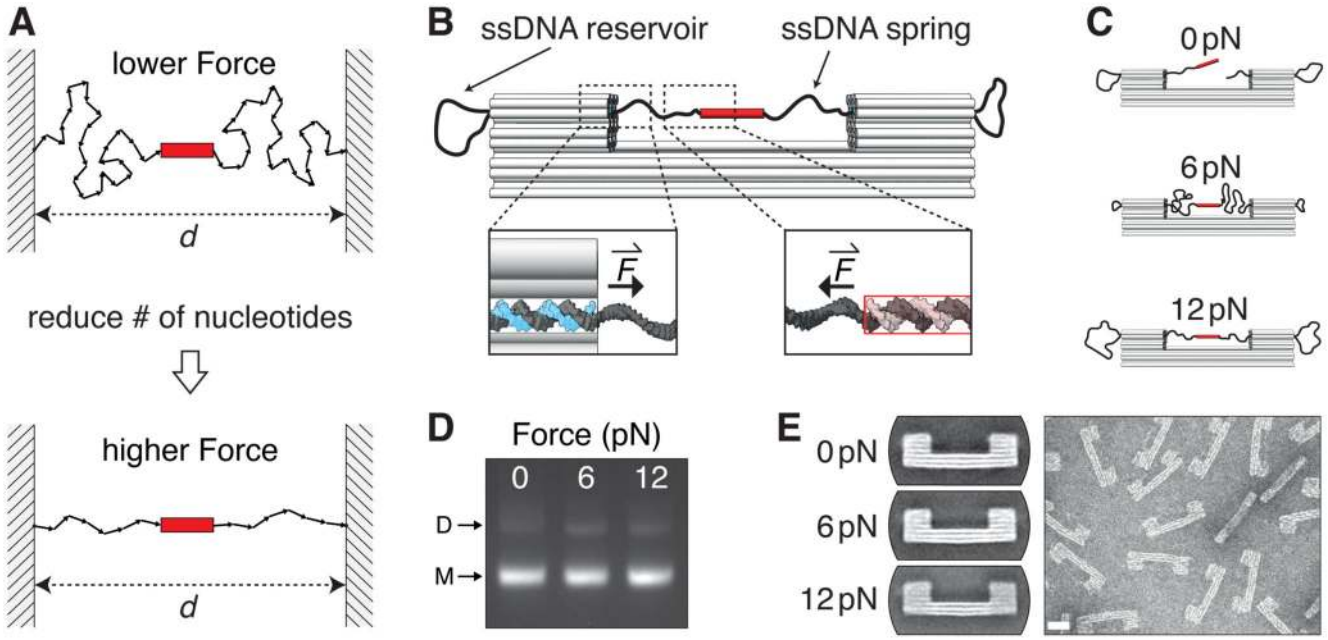

Fig. 1. DNA origami force clamp.

(**A**) ssDNA connects the molecular system of interest (red rectangle) with two immobile anchor points. Reducing the number of nucleotides spanning the distance *d* leads to a smaller number of adoptable conformations of the ssDNA chain and thus results in a higher entropic force. (**B**) Scheme of the DNA origami force clamp structure. ssDNA exits the clamp duplexes in a shear conformation (left inset: scaffold in black, staple in blue) and spans the 43 nm wide gap. ssDNA reservoirs are located on each side of the clamp. The system of interest (here a DNA duplex) is probed in shear conformation (right inset). (**C**) For each constant force variant (three variants are shown here), individual origami samples were assembled. (**D**) Agarose gel of the three variants after annealing with the monomer (M) and dimer band (D) of the origami structure highlighted. (**E**) Average TEM micrographs of the three variants (left) and single negative-stain TEM image of the 6 pN variant (right). Scale bars: 20 nm.

Europe PMC Funders Author Manuscripts

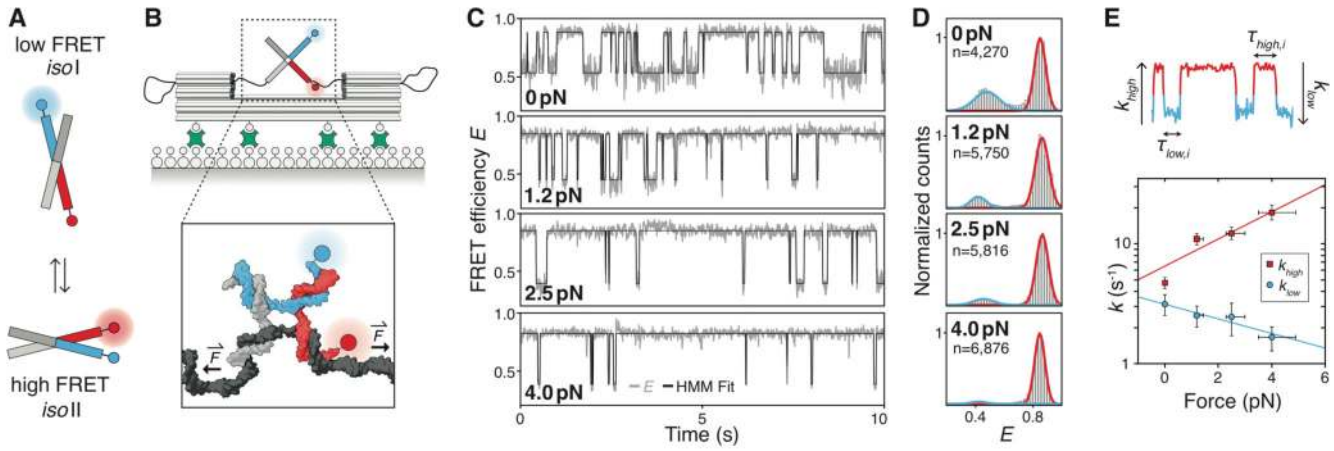

Fig. 2. Holliday junction conformer transitions under force.

(**A**) Schematics of the HJ switching between two stacked isomers; Cy3 donor (blue) and Cy5 acceptor (red). (**B**) Force clamps were immobilized on a BSA-covered glass surface via biotin-streptavidin coupling. The HJ system is mounted in the force clamp with one of the four HJ-strands being the scaffold (black strand in inset). (**C**) FRET traces with the FRET efficiency E (gray line) and two-state hidden Markov fit (black line). (**D**) Histograms over all recorded FRET traces with Gaussian fits for the two FRET populations in blue (low-FRET) and red (high-FRET). Only traces with > 20 transitions were included in the analysis; n is the total number of transitions. (**E**) Dwell times for both states ($\tau_{low,i}$, $\tau_{high,i}$) were extracted for each trace. Transition rates (k_{low}, k_{high}) were first extracted from a mono-exponential decay fit for each dwell time histogram, then averaged and plotted (semi-log plot) as a function of force. Red squares: low- to high-FRET (k_{high}); blue circles: high- to low-FRET (k_{low}). Solid lines are exponential fits where the exponent relates rates to the applied force. Y-axis error is the standard error of each average rate; x-axis error is the uncertainty of the calculated force (fig. S15)

Europe PMC Funders Author Manuscripts

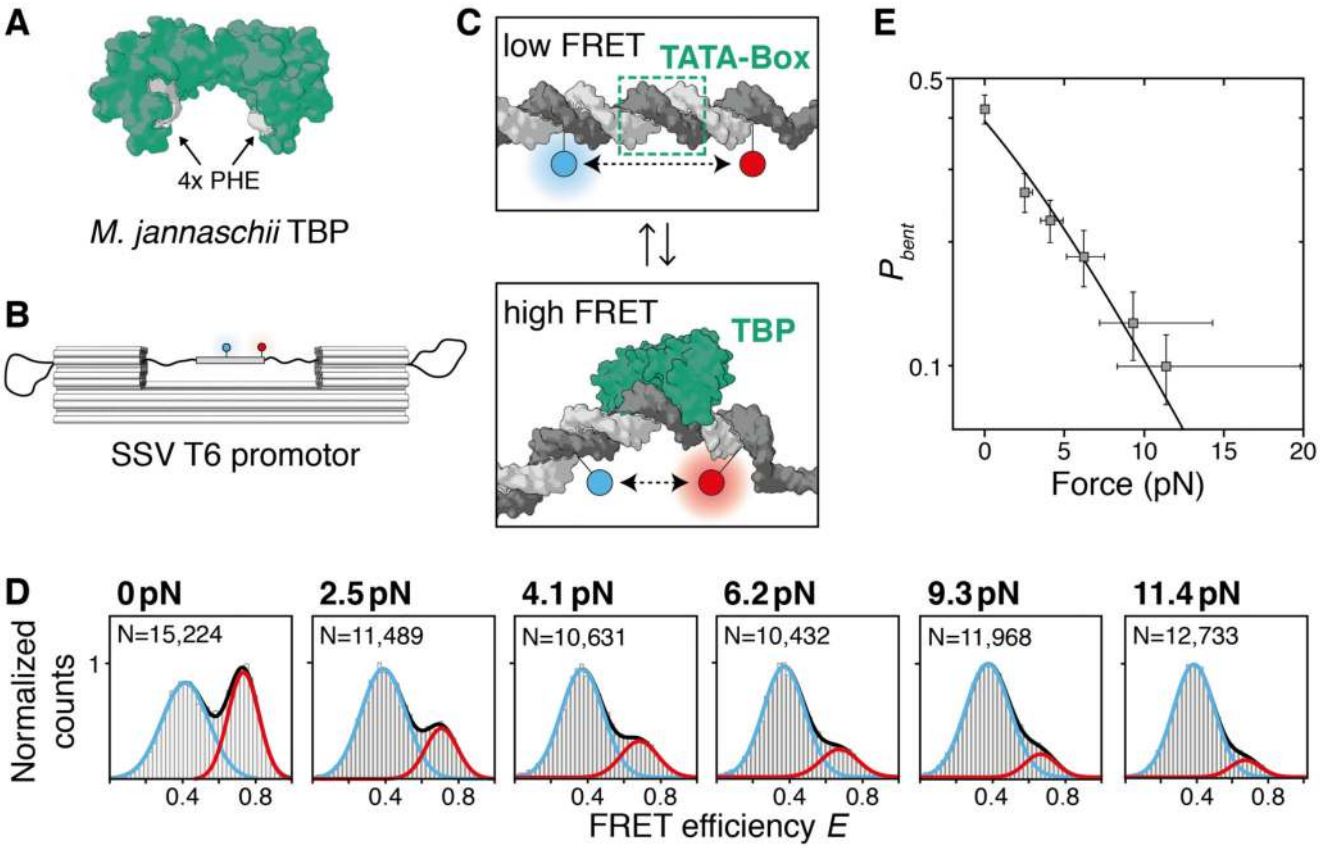

Fig. 3. TBP-induced DNA bending under force.

(**A**) TBP from *M.jannaschii* (PDB: 2Z8U) (29). Two pairs of phenylalanines located in the DNA binding domain promote DNA bending. (**B**) The SSV T6 promotor including the TATA-box mounted on the force clamp; Atto532 donor (blue) and Atto647n acceptor (red). (**C**) TBP binds the minor groove of the TATA-box and bends the duplex by almost 90°, thus changing the distance between donor and acceptor. (**D**) FRET histograms and Gaussian fits for the low-FRET (blue) and high-FRET (red) population. *N* is the number of molecules measured for each force. (**E**) Semi-log plot of the probability of the bent state P_{bent} as a function of force. The solid line is a Boltzmann distribution fit. Y-axis error is the standard error of P_{bent}; x-axis error is the uncertainty of the calculated force (fig. S28).

Europe PMC Funders Author Manuscripts